The Journal of Neuroscience, October 1, 1998, *18*(19):7613–7624

Dendritic Hyperpolarization-Activated Currents Modify the Integrative Properties of Hippocampal CA1 Pyramidal Neurons

Jeffrey C. Magee

Neuroscience Center, Louisiana State University Medical Center, New Orleans, Louisiana 70112

Step hyperpolarizations evoked slowly activating, noninactivating, and slowly deactivating inward currents from membrane patches recorded in the cell-attached patch configuration from the soma and apical dendrites of hippocampal CA1 pyramidal neurons. The density of these hyperpolarization-activated currents (I_h) increased over sixfold from soma to distal dendrites. Activation curves demonstrate that a significant fraction of I_h channels is active near rest and that the range is hyperpolarized relatively more in the distal dendrites. I_h activation and deactivation kinetics are voltage-and temperature-dependent, with time constants of activation and deactivation decreasing with hyperpolarization and depolarization, respectively. I_h demonstrated a mixed Na^+–K^+ conductance and was sensitive to low concentrations of external CsCl. Dual whole-cell recordings revealed regional differences in input resistance (R_{in}) and membrane polarization rates (τ_{mem}) across the somatodendritic axis that are attributable to the spatial gradient of I_h channels. As a result of these membrane effects the propagation of subthreshold voltage transients is directionally specific. The elevated dendritic I_h density decreases EPSP amplitude and duration and reduces the time window over which temporal summation takes place. The backpropagation of action potentials into the dendritic arborization was impacted only slightly by dendritic I_h, with the most consistent effect being a decrease in dendritic action potential duration and an increase in afterhyperpolarization. Overall, I_h acts to dampen dendritic excitability, but its largest impact is on the subthreshold range of membrane potentials where the integration of inhibitory and excitatory synaptic inputs takes place.

Key words: hyperpolarization-activated current; dendrite; hippocampus; synaptic integration; CA1 pyramidal neuron; action potential backpropagation

The primary site of excitatory synaptic input into hippocampal pyramidal neurons is the vast dendritic arborization that comprises >95% of the membrane surface area of the cell. Here in the dendrites, information received from tens of thousands of synaptic inputs is coordinated and stored via the highly complex processes of dendritic integration and synaptic plasticity. It is now well known that a rich variety of voltage-gated ion channels bestows on dendrites unique active properties that impact all aspects of dendritic function (Yuste and Tank, 1996; Stuart et al., 1997; Magee et al., 1998).

Although the relative densities and key biophysical characteristics of several Na^+, K^+, and Ca^{2+} channel types have been reported for CA1 pyramidal neurons (Magee and Johnston, 1995; Hoffman et al., 1997), very little is known about hyperpolarization-activated (I_h) channels in CA1 dendrites. I_h plays a variety of important roles in many neuronal and nonneuronal cell types (for review, see Pape, 1996) and has been reported to be present in CA1 pyramidal neurons (Halliwell and Adams, 1982; Maccaferri et al., 1993; Gasparini and DiFrancesco, 1997). Various membrane parameters (input resistance, membrane time constant, and resting potential) as well as general membrane phenomena (rectification, oscillatory activity, and action potential firing rates) are all modulated by I_h (Mayer and Westbrook, 1983; Spain et al., 1987; Pape and McCormick, 1989; Maccaferri et al., 1993; Maccaferri and McBain, 1996; Gasparini and DiFrancesco, 1997). Thus, the presence of I_h in the dendrites of CA1 pyramidal neurons potentially could have a significant impact on the dendritic integration of subthreshold synaptic activity and the propagation of action potentials.

The basic biophysical properties and the subcellular distribution of I_h were investigated in hippocampal CA1 pyramidal neurons, using cell-attached and outside-out patch-clamp techniques. The impact of these channels on the shape and propagation of subthreshold voltage signals and action potentials also was determined by using simultaneous whole-cell voltage recordings from both the soma and dendrites.

MATERIALS AND METHODS

Hippocampal slices (400 μm) were prepared from 5- to 16-week-old Sprague Dawley rats, using standard procedures that have been described previously (Magee et al., 1996). Pyruvic acid (3 mM) and ascorbic acid (1 mM) were added to both the perfusion and incubation solutions. Individual neurons were visualized with a Zeiss Axioskop microscope (Oberkochen, Germany) fit with differential interference contrast (DIC) optics, using infrared illumination. All neurons exhibited resting membrane potentials between −62 and −75 mV.

For channel recordings the bath solutions contained (in mM): 125 NaCl, 2.5 KCl, 1.25 NaH_2PO_4, 25 $NaHCO_3$, 2.0 $CaCl_2$, 1.0 $MgCl_2$, and 25 dextrose. The external solution was bubbled with 95% O_2/5% CO_2 at 23 or 33°C, pH 7.4, for all recordings. The standard cell-attached recording pipette solution consisted of (in mM): 120 KCl, 10 HEPES, 2.0 $CaCl_2$, 1.0 $MgCl_2$, 20 tetraethylammonium-Cl (TEA-Cl), 5.0 4-aminopyridine (4-AP), and 1 $BaCl_2$, pH 7.4 with KOH. The "physiological" cell-attached recording pipette solution consisted of (in mM): 110 NaCl, 10 HEPES, 2.5 KCl_2, 2.0 $CaCl_2$, 1.0 $MgCl_2$, 30 TEA-Cl, 5.0 4-AP, and 1 $BaCl_2$, pH 7.4 with NaOH. For outside-out patch recordings the pipette solution consisted of (in mM): 120 $KMeSO_4$, 20 KCl, 10 HEPES, 10 EGTA, 4.0 Mg_2-ATP, 0.3 $Tris_2$-GTP, 14 phosphocreatine, and 4 NaCl, pH 7.25 with KOH. Pipettes were pulled from borosilicate glass (9–12 MΩ) and coated with Sylgard. The tips were inspected

Received April 15, 1998; revised July 9, 1998; accepted July 10, 1998.

This work was supported by National Institutes of Health Grant NS35865. I thank Michael Carruth for technical assistance.

Correspondence should be addressed to Dr. Jeffrey C. Magee, Neuroscience Center, Louisiana State University Medical Center, 2020 Gravier Street, New Orleans, LA 70112. E-mail: jmagee@lsumc.edu

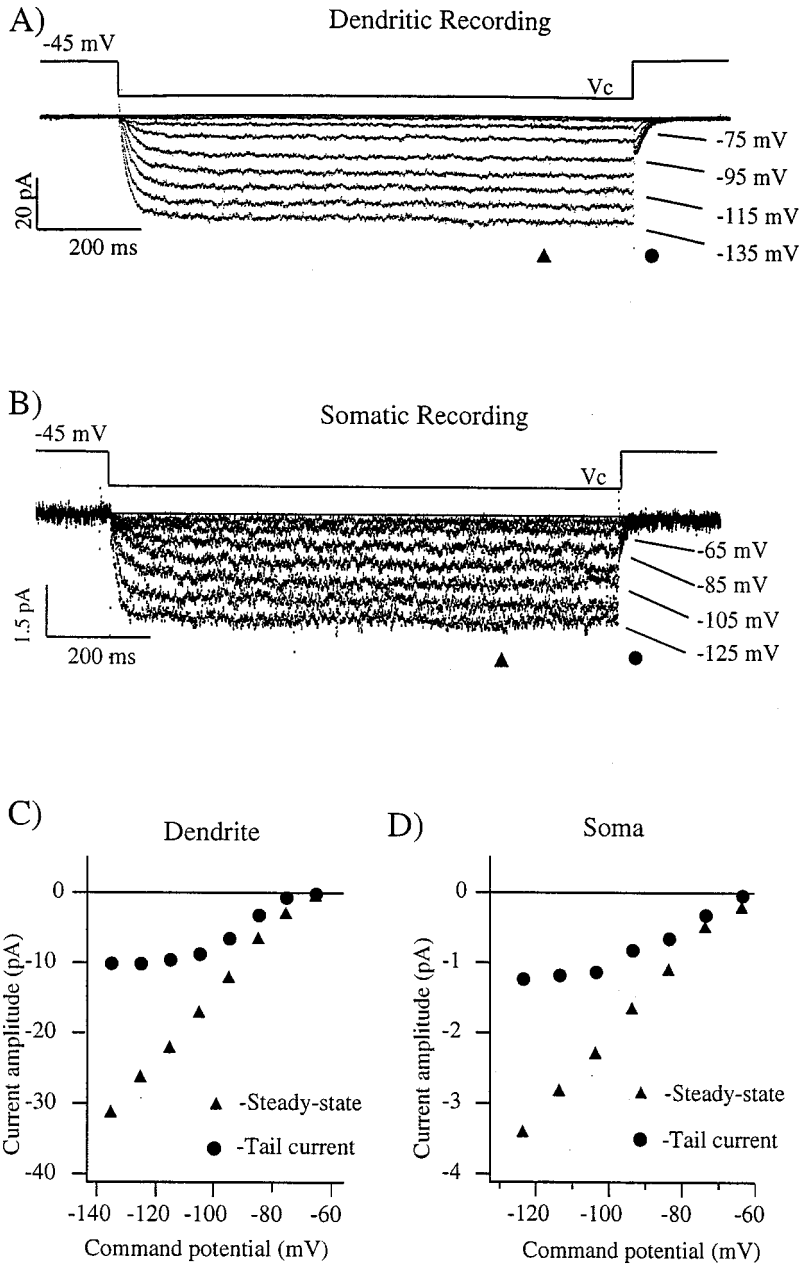

Figure 1. Step hyperpolarizations (1 sec duration) evoke slowly activating and noninactivating inward currents from cell-attached patches located in the apical dendrites (*A*) and somata (*B*) of CA1 pyramidal neurons. *C*, *D*, Current–voltage relationships for the recordings that are shown *above*. Steady-state current amplitudes (*filled triangles*) are the averages of all points at 900–910 msec after the start of hyperpolarizing step. Tail current amplitudes (*filled circles*) are the averages of all points at 4.5–5.5 msec after repolarization. The holding potentials and series of command potentials (V_c) are shown in the figure. Bath temperature was 33°C for all of the recordings shown. The number of points in each trace has been reduced by one-half for clarity.

visually before use and had uniform tip diameters of ~1 μm for both dendritic and somatic recordings. Channel recordings, using an Axopatch 200B amplifier (Axon Instruments, Foster City, CA), were analog-filtered at 1 or 2 kHz and digitally filtered at 1 or 0.5 kHz off-line. Leakage and capacitive currents were subtracted digitally by scaling traces evoked by steps from −20 to −50 mV.

All curve fitting (I_h activation and deactivation time constants, activation curves, voltage decays, and various *x*–*y* plots) was performed with a least-squares program (IgorPro, WaveMetrics, Lake Oswego, OR). Activation curves are least-square fits of the data to a Boltzmann function. CsCl (Sigma, St. Louis, MO) was added to a solution identical to the standard cell-attached solution and was applied to the excised patch via a small-bore perfusion pipette. Error bars represent SEM, and the number of patches (*n*) is given in parentheses.

Whole-cell patch-clamp recordings were made by using two Dagan (Minneapolis, MN) BVC-700 amplifiers in active "bridge" mode. The external recording solution contained (in mM): 124 NaCl, 2.5 KCl, 1.2 NaH_2PO_4, 25 $NaHCO_3$, 2.0 $CaCl_2$, 1.5 $MgCl_2$, 10 dextrose, and 0.005 DNQX, bubbled as above at ~35°C, pH 7.4. Whole-cell recording pipettes (somatic, 2–4 MΩ; dendritic, 5–7 MΩ) were pulled from borosilicate glass. The internal solution was the outside-out patch recording solution with the addition of 0.5 mM EGTA. Series resistance for somatic recordings was 6–20 MΩ, whereas that for dendritic recordings was 15–40 MΩ. Dendritic pipettes were coated with Sylgard. Voltages have not been corrected for the theoretical liquid junction potentials (6–7 mV).

RESULTS

Hyperpolarization-activated inward current

Long-duration (1–3 sec) step hyperpolarizations evoked inward currents from cell-attached patches obtained from both the somatic and apical dendritic regions of hippocampal CA1 pyramidal neurons (Fig. 1*A,B*). These inward currents were slowly activating, noninactivating, and slowly deactivating. In general, patches were held 20 mV depolarized to the resting potential (soma: −67 ± 2 mV, $n = 15$; >100 μm dendrite: −70 ± 2 mV, $n = 18$), which was determined by patch rupture after the recording period. Currents began activating near −60 mV, and steady-state

current amplitude increased in an approximately linear manner for the membrane potentials that were tested (up to −140 mV). On the other hand, tail current amplitude (recorded at approximately −50 mV) peaked after steps to approximately −100 mV (Fig. 1*C,D*). These general features of hyperpolarization-activated currents were found in both somatic and dendritic recordings. For the majority of I_h recordings a high external K^+ recording solution was used because the greatly increased current amplitude provided by such a solution (DiFrancesco, 1981; Mayer and Westbrook, 1983; Spain et al., 1987; Maruoke et al., 1994) allowed for an accurate comparison of I_h properties and distribution over a large part of the somatodendritic axis of the neurons.

Subcellular distribution

I_h was observed in all regions of CA1 pyramidal neurons from which recordings were obtained, including regions of the apical dendrite located in the most distal stratum radiatum and proximal stratum moleculare (Fig. 2*A*). Steady-state current amplitude at approximately −130 mV progressively increased with distance away from the soma (soma: 8.9 ± 1.6 pA, $n = 21$; 300–350 μm dendrite: 62.3 ± 8.5 pA, $n = 14$). The mean current could be converted to mean current density (per μm^2) by normalizing to an ~5 μm^2 patch area (Magee and Johnston, 1995) and was 1.8 ± 0.3 pA/μm^2 ($n = 21$) at the soma as compared with a density of 12.5 ± 1.7 pA/μm^2 ($n = 14$) recorded from dendrites located 300–350 μm away from the soma (Fig. 2*B*, Tables 1, 2). Maximum I_h conductance (from the fully activated tail current recorded at approximately −50 mV, using a reversal potential of 0 mV) increased from 63.6 ± 12.2 pS ($n = 6$) at the soma to 429.7 ± 87.2 pS ($n = 7$) 300–350 μm out in the dendrites. For all of these measures this is an approximately sevenfold increase across the somatodendritic axis. Single I_h channel activity was too small to be measured accurately with the noise levels (no less than 300 fA RMS, 5 kHz) present in these experiments.

I_h amplitude was reduced significantly when external recording solutions contained 60 mM Na^+/60 mM K^+. In this solution the mean current amplitude was 22.6 ± 6.2 pA at −130 mV (all dendritic recordings were from ~300 μm; $n = 9$), which is reduced to nearly one-third of the mean current amplitude recorded at the same dendritic location in 0 Na^+ external (54.6 ± 7.6 pA, 130 mV; $n = 10$). Current amplitude was reduced even further when the external recording solution contained more physiological K^+ (2.5 mM) and Na^+ (110 mM) concentrations (4.5 ± 1.1 pA, −130 mV; $n = 3$; ~300 μm). Using a range of reversal potentials from −20 to −40 mV (Pape, 1996), we can calculate a conductance density estimate of 8–10 pS/μm^2 for the distal dendritic regions. Using the density decrease reported in Figure 2*B*, we can infer a 1–2 pS/μm^2 for the somatic compartment. The dendritic I_h conductance density would be ~10-fold lower than the conductance density previously reported for Na^+ channels located in the distal dendritic regions (Magee and Johnston, 1995). Na^+ channel recordings made from the same patches as above (with 110 mM Na^+) would support this estimate (Fig. 2*C*).

Voltage ranges of activation

Activation curves were generated by using the slowly decaying tail currents present on membrane repolarization (to approximately −50 mV) from the command potential (Fig. 3*A,B*). Tail current amplitude was measured at ~5 msec after step repolarization, allowing for the complete decay of any residual capacitive current. Recordings obtained from dendritic membrane (>100 μm away from soma) presented a voltage range of activation ($V_{1/2}$ = −89.5 ± 1.0 mV; $k = 8.5 \pm 0.5$; $n = 13$) that was shifted in a hyperpolarized direction as compared with that obtained from the more proximal regions of the neuron ($V_{1/2} = -81.9 \pm 1.2$ mV; $k = 8.8 \pm 0.5$; $n = 10$) (<100 μm) (Fig. 3*C*). These voltage ranges determine that ~10% of the maximal current is activated at rest in the soma, whereas somewhat less (~5%) relative channel activation occurs at rest in the more distal dendrites for the 0 mM

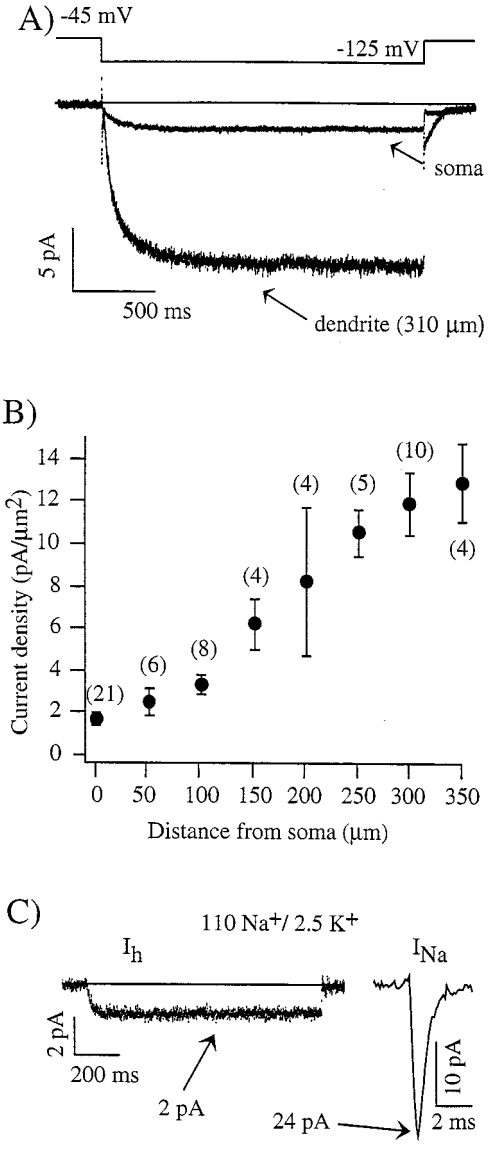

Figure 2. Hyperpolarization-evoked current amplitude increases with distance from soma. *A*, In a cell-attached patch located in the apical dendrites (310 μm), steps from −45 to −125 mV evoked inward currents were approximately sixfold larger than those recorded from the soma of the same CA1 pyramidal neuron. *B*, Plot of mean current amplitude (at −125 to −130 mV), normalized to patch area, for recordings across the somatodendritic axis. The *number* of recordings for each point is shown in *parentheses*. Error bars indicate SEM. *C*, I_h evoked by a step hyperpolarization from −50 to −130 mV in physiological recording solution. The patch is located ~315 μm from the soma. On the *right* side of the figure is the peak Na^+ current evoked in the same patch by a step from −90 to −10 mV, which is used for comparison. Bath temperature was 22°C for recordings shown in *A* and 33°C for those in *C*. The number of points in each I_h trace has been reduced by one-half for clarity.

Table 1. Hyperpolarization-activated current parameters

	Density[a] (pA/μm²)	$V½$ (mV)	K (mV)	Act. τ[a] (msec)	Deact τ[b] (msec)	E_{rev} (mV)
Soma	1.8 ± 0.3 (20)	−82 ± 1.2 (10)	8.8 ± 0.5 (10)	17 ± 2.1 (6)	18 ± 0.2 (6)	−2 ± 1.9 (4)
Dendrite	11.9 ±1.5 (9)	−90 ± 1.0 (14)	8.5 ± 0.5 (14)	20 ± 1.4 (7)	16 ± 0.8 (9)	+1 ± 2.4 (5)
Na ext.[c]	4.5 ± 1.3 (9)	−81 ± 1.3 (6)	7.0 ± 0.7 (6)	19 ± 2.8 (5)	26 ± 2.2 (5)	−13 ± 4.0 (8)

[a] At approximately −120 mV, dendrite at approximately 250 μm; [b] at approximately −45 mV; [c] 250 μm dendritic recordings in solution with 60 mM Na^+.

Table 2. Membrane and EPSP properties

	R_{in}[a] (MΩ)	Repol. τ[b] (msec)	Single EPSP amplitude (mV)	EPSP train amplitude (mV)	Propagation (%)[c]	V_m (msec)
Soma	66 ± 5 (13)	28 ± 4 (13)	2.8 ± 0.2 (6)	8.4 ± 0.9 (6)	49 ± 5 (6)	−67 ± 2 (10)
Soma+Cs	112 ± 6 (13)	42 ± 10 (13)	3.1 ± 0.4 (6)	11.7 ± 0.8 (6)	76 ± 6 (6)	−72 ±2 (10)
Dendrite[d]	39 ± 2 (13)	15 ± 2 (13)	7.9 ± 0.5 (6)	23.9 ± 2.9 (6)	79 ± 4 (6)	−69 ± 1 (11)
Dend + Cs^+	100 ± 3 (13)	27 ± 5 (13)	8.8 ± 0.6 (6)	29.0 ± 2.7 (6)	77 ± 5 (6)	−73 ± 2 (11)

[a] Measured from current injections ranging from −50 to +50 pA; [b] measured after an ~10 mV depolorization; [c]Soma is from soma to dendrite; dendrite is from dendrite to soma, −100 pA current injection; [d]dendritic recordings from 250 to 300 μm; $+Cs^+$ is with bath application of 3 mM CsCl. EPSP is voltage-transient in response to exponential dendritic current injection.

Na^+ solutions. The hyperpolarized shift in the dendritic activation curve thus reduces the impact of the extremely elevated distal dendritic channel density on resting membrane properties.

The presence of Na^+ in the external solution (10–60 mM) shifted the activation curve of dendritic channels nearly 10 mV in a depolarized direction ($V_{1/2}$ = −80.5 ± 1.3 mV; k = 6.7 ± 0.7; n = 6) (see Fig. 6*C*). Proximal currents were too small in amplitude to generate accurate activation curves, but they too appeared to be shifted similarly. This indicates that under more physiological conditions ~25% of hyperpolarization-activated channels would be open at rest in the soma, whereas nearly one-half this much would be activated in the distal regions of the neuron.

Activation and deactivation kinetics

For both dendritic and somatic recordings the rate of current activation was voltage-dependent such that the activation time constant decreased with increasing hyperpolarization (from ~50 msec at −75 mV to ~16 msec at −125 mV; Fig. 4*A,C*). These time constants were recorded with a bath temperature of 33°C. In five recordings the temperature of the bathing solution was reduced from 33 to 23°C, and activation time constants slowed from 17.8 ± 1.3 to 80.2 ± 10.7 msec. Thus, activation has a Q_{10} of 4.5. There was very little differences observed between the activation kinetics of somatic versus dendritic currents, although somatic activation may have been slightly faster at the most negative potentials (Fig. 4*C*).

Current deactivation was also voltage- and temperature-dependent. Tail current decay time constants decreased with increasing depolarization (30 msec at −70 mV to ~7 msec at −30 mV; 33°C; Fig. 4*B,C*). Deactivation kinetics were also temperature-dependent, going from 14.4 ± 2.0 to 68.2 ± 9.8 msec when the bathing solution was reduced from 33 to 23°C (Q_{10} = 4.7; n = 5). As with other channel types the temperature dependence of current amplitude was much lower (Q_{10} = 1.95; n = 5).

Although single I_h channel activity has been reported in sinoatrial (SA) node cells (DiFrancesco, 1986), there still remains some possibility that I_h is not a classically voltage-gated channel and that I_h perhaps may be mediated by some type of ion carrier. Although the noise levels in the present recordings did not allow for the observation of single channel activity (the reported single channel conductance is <1 pS), the temperature dependence exhibited by the currents is very similar to that observed for other voltage-gated ionic channels (Byerly et al., 1984; van Lunteren et al., 1993; Haverkampf et al., 1995; McAllister-Williams and Kelly, 1995; Milburn et al., 1995). The gating kinetics of voltage-gated ion channels generally show Q_{10} at ~5, whereas the Q_{10} of current amplitude is generally <2. The difference in these values results from differences in the thermodynamics of channel gating, which is more similar to that of enzyme reactions, whereas channel permeation shows a lower temperature sensitivity as a result of being a more diffusion-like process (van Lunteren et al., 1993). I_h, therefore, exhibits thermodynamic properties that are more similar to those of voltage-gated ion channels instead of some ion carrier for which both the kinetics and current amplitude would present similar Q_{10}.

The presence of Na^+ in the external solution (10–60 mM) did not affect the activation kinetics but did slow channel deactivation ~83% (τ = 26.3 ± 2.2 msec at −50 mV; 33°C; n = 5) (see Fig. 5*A,B*). The Q_{10} values given above were not affected by the change in external [Na^+]. The ability of external Na^+ to slow channel deactivation has been observed in SA node cells and was attributed to the presence of an external Na^+ binding site capable of modulating channel gating (Maruoke et al., 1994). Perhaps a similar mechanism is present in I_h here and also may be responsible for the depolarizing shift in the voltage range of activation observed in Na^+ containing external solutions.

Ionic composition

Reversal potentials determined from fully activated instantaneous *I–V* relationships were used to estimate the ionic selectivity of hyperpolarization-activated currents in CA1 pyramidal neurons (Fig. 6). With external solutions containing 120 mM K^+, the instantaneous *I–V* relationship reversed at −1 ± 2.1 mV (n = 9; no difference was observed between somatic and dendritic recordings, so the data were pooled). With external solutions containing 60 mM Na^+/60 mM K^+, the reversal potential shifted 12 mV hyperpolarized (−13 ± 4; n = 8). From the mean reversal potentials a Na^+/K^+ permeability ratio of ~0.35 could be determined with the Goldman–Hodgkin–Katz equation. These data indicate that I_h has a mixed ionic conductance with significant permeabilities to both Na^+ and K^+. It should be noted that, because I_h conductance has been reported to vary significantly

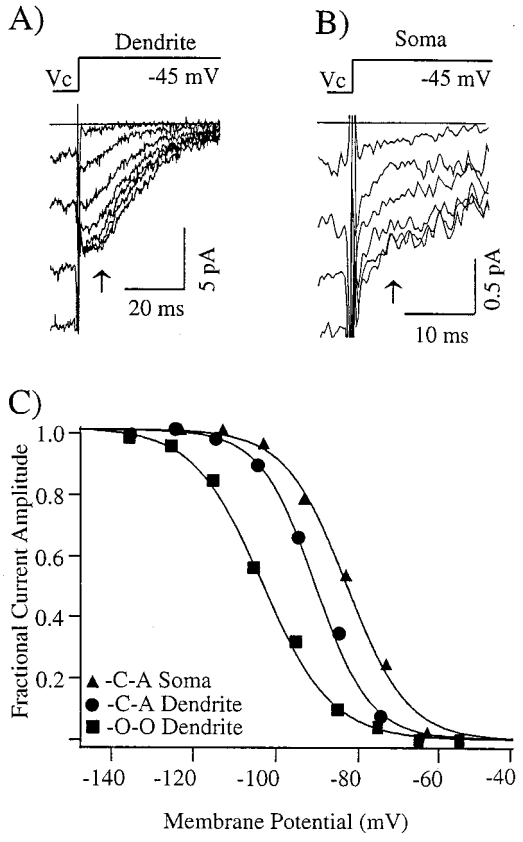

Figure 3. Voltage ranges of activation for dendritic channels are shifted in a hyperpolarized direction, as compared with those located at the soma. The slow deactivation of hyperpolarization-activated currents allows activation curves to be generated directly from the tail currents that are present after repolarization from command potentials (V_c). Representative tail currents are shown for cell-attached patches located in the dendritic (310 μm) (*A*) and somatic regions (*B*) of CA1 pyramidal neurons. *Arrows* indicate locations at which the tail current amplitude was measured. *C*, Activation curves generated from the currents that are shown *above*. The dendritic curve ($V_{1/2} = -89$ mV; $k = 6$; *filled triangles*) is shifted 6 mV hyperpolarized with respect to the somatic curve ($V_{1/2} = -83$ mV; $k = 7$; *filled circles*). Slope factors (k) for the two curves are similar. A representative activation curve for a patch recorded in the outside-out configuration ($V_{1/2} = -102$ mV; $k = 8$; *filled squares*) also is shown for comparison. Command potentials (V_c) were given in 10 mV increments from −65 to −135 mV in *A* and from −65 to −125 in *B*. Bath temperature was 33°C for all of the recordings shown.

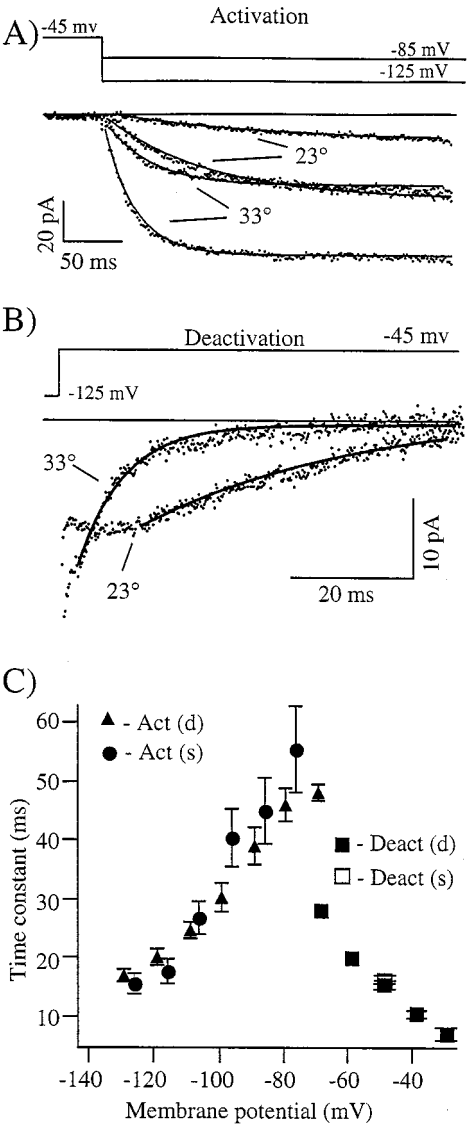

Figure 4. Activation and deactivation kinetics are highly temperature-dependent. *A*, The activation rate of currents evoked by step hyperpolarizations from −45 to −85 and to −125 mV increases nearly fivefold for a 10°C increase in bath temperature. Curves are well fit by single exponential functions (*solid lines*). *B*, The deactivation rate of currents present after repolarization from −125 to −45 show a similar temperature dependence. After a short plateau region the current decays are well fit by single exponential functions (*solid lines*). *C*, Plot of activation time constants as a function of command potential for both dendritic (*filled triangles*) and somatic recordings (*filled circles*). Deactivation time constants for a range of membrane potentials are shown for dendritic recordings (*filled squares*) and for somatic recordings (*open squares*) at a single potential. Holding and command potentials are shown in the figure. The currents that are shown are from a single dendritic recording (260 μm). The number of points in each trace in *A* has been reduced to 1/8 for clarity.

from the independence principle (Wollmuth, 1995), the permeability ratios given here are only approximations.

The effect of external Na^+ on current amplitude fits well with the idea that the I_h channel is a multi-ion pore possessing high-affinity binding sites for both Na^+ and K^+. That the addition of a few millimolars concentration of Na^+ to the external recording solution was capable of decreasing the current amplitude to a much greater extent than would be expected from changes in reversal potential can be explained by the anomalous mole fraction mechanism described for many other channel types (including I_h) (Hille, 1992; Wollmuth, 1995).

External Cs^+ blockade

Inclusion of Cs^+ in the high K^+ external recording solution reduced the peak hyperpolarization-activated current amplitude in a concentration-dependent manner. Current kinetics were not affected by external Cs^+. Cs^+ (0.3 mM) reduced the hyperpolarization-activated current amplitude to ~0.5 that of control, whereas 5 mM Cs^+ produced a nearly complete channel blockade (Fig. 7).

Physiology

Input resistance

Dual whole-cell recordings from the soma and distal dendrites of the same neuron were used to determine the effect of the differential distribution of I_h channels on basic membrane properties

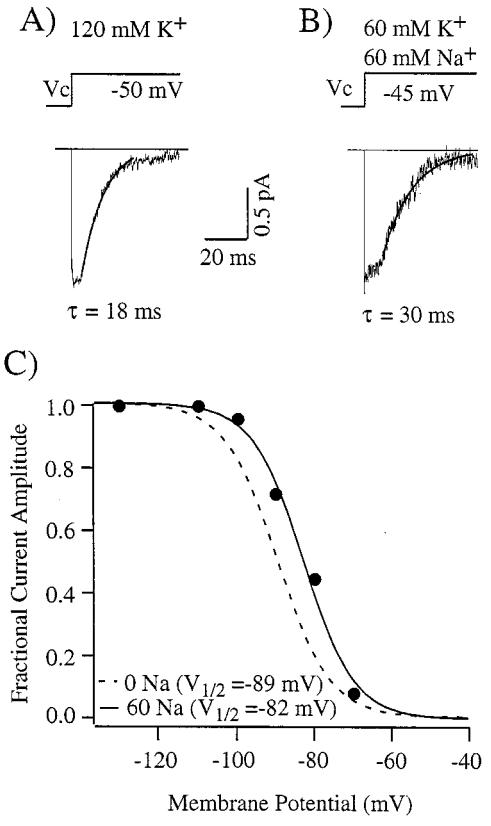

Figure 5. The presence of external Na^+ slows the deactivation rate and shifts the voltage range of activation of hyperpolarization-activated currents. *A*, Current relaxations after a step depolarization from −130 to −50 mV with 0 Na^+ in external solution. The current is well fit by a single exponential function (τ is shown). *B*, Current relaxations after a step depolarization from −125 to −45 mV with 60 mM Na^+ in external solution, showing slowed deactivation kinetics. The current is well fit by a single exponential function (τ is shown). *C*, Voltage range of activation for the patch that is shown *above* in the presence of 60 mM external Na^+. The *dashed line* is a representative activation curve for hyperpolarization-activated current with 0 mM external Na^+. External Na^+ shifts the activation range nearly 10 mV depolarized, without any obvious effect on *k*. The currents that are shown are from two different dendritic recordings at 33°C.

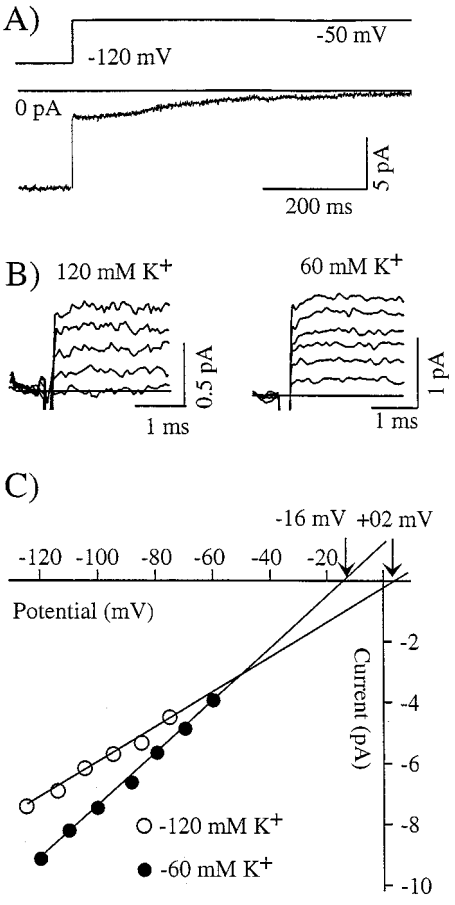

Figure 6. Reversal potential of hyperpolarization-activated currents indicates mixed ion conductance. *A*, Current relaxation after a step depolarization from approximately −120 to −50 mV. *B*, *Left*, Current relaxations shown at a faster time scale for conditions in which 120 mM K^+/0 mM Na^+ was present in the external pipette solution for potentials ranging from −125 to −85 mV. *B*, *Right*, Current relaxations shown for conditions in which 60 mM K^+/60 mM Na^+ was present in the external pipette solution for potentials ranging from −120 to −70 mV (from the same recording as in *A*). *C*, Current–voltage relationships for the above currents. Reversal potentials for the two conditions are indicated on the plot. The currents that are shown are from two different dendritic recordings at 23°C.

and the subcellular propagation of potentials. As would be expected, hyperpolarizing current injections (300 msec duration) caused substantially reduced voltage deflections in the dendritic compartments (11 ± 1 mV peak; 8 ± 1 mV steady-state; $n = 13$; −200 pA) when compared with the somatic compartment (15 ± 2 mV peak; 13 ± 1 mV steady-state; $n = 13$; −200 pA) (Fig. 8*A,B*). Input resistances (R_{in}) were calculated as the slope of the current–voltage relationship for current injections ranging from −50 to +50 pA; a R_{in} of 39 ± 2 MΩ was calculated for dendrites as compared with 66 ± 5 MΩ for somata (Fig. 8*E,F*). Peak depolarizing voltage deflections in response to 300 msec, +100 pA current injections likewise were reduced in the dendritic compartments (4 ± 1 mV; $n = 13$) as compared with the somatic compartments (6 ± 2 mV; $n = 13$).

The blockade of ~80% of I_h by bath application of 3 mM Cs^+ increased R_{in} in all regions of the neuron and greatly reduced the regional differences in R_{in} (dendrite: 100 ± 3 mΩ, $n = 13$; soma: 112 ± 6 mΩ, $n = 13$) (Fig. 8*C,D*). The increase in R_{in} observed under I_h blockade significantly increased the excitability of the neuron such that previously subthreshold current injections (100–200 pA, either dendritic or somatic) could now evoke repetitive action potential firing (Fig. 8*C*). Application of external Cs^+ also caused a slight hyperpolarization in resting membrane potential that was similar in both the proximal and distal regions of the neuron (dendrite: −4 ± 0.4 mV, $n = 11$; soma: −5 ± 0.7 mV, $n = 10$). In all cases a depolarizing current was injected to compensate for this change in membrane potential.

Subthreshold potential propagation

As a result of the regional R_{in} differences the propagation of subthreshold potentials is directionally specific. In general, there is a greater amount of decrement in voltage signals as they propagate from the soma to the dendrites (decrease to 49 ± 5%, $n = 6$, 250–300 μm) (Fig. 9*A–C*, *open diamonds*) than from the dendrites to the soma (decrease to 79% ± 4%, $n = 6$, 250–300 μm). Also, the progressively lower R_{in} of the dendritic compartment increasingly dampens voltage changes such that the amplitude of the dendritic voltage change in response to a dendritic current injection (termed the *local* dendritic signal) decreases

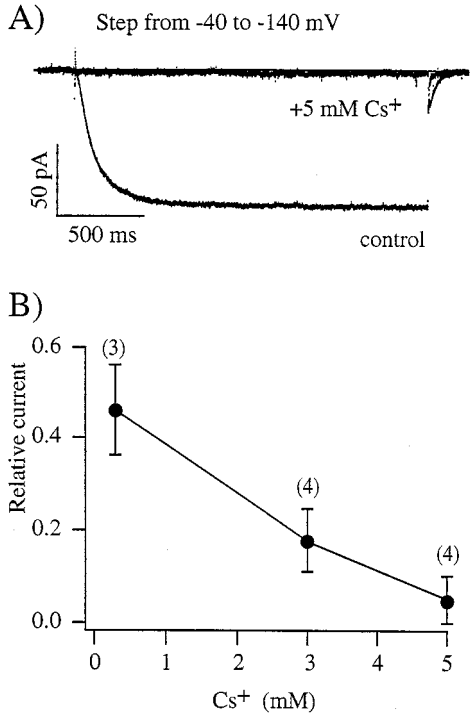

Figure 7. External CsCl blocks hyperpolarization-activated currents. *A*, Currents activated by step hyperpolarizations from −40 to −140 mV under control conditions and in the presence of 5 mM CsCl in the external solution (high K^+). In this patch, 5 mM Cs blocked >95% of the evoked current. *B*, Plot of relative current remaining after wash-in of a solution containing three different concentrations of Cs^+. The currents that are shown are from a dendritic patch in an outside-out configuration at 23°C. The number of points in each trace has been reduced by one-half for clarity.

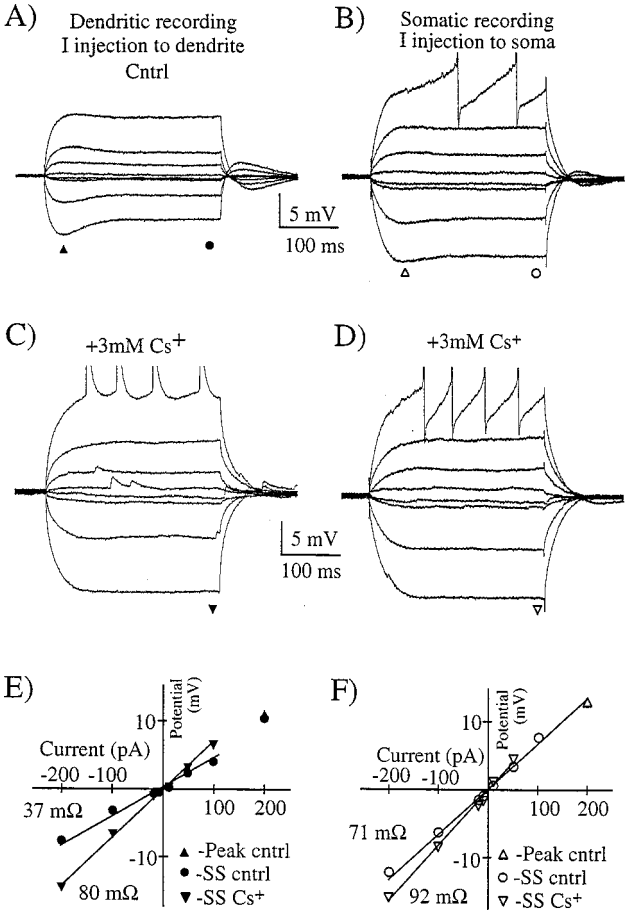

Figure 8. I_h generates a spatially nonuniform input resistance. *A*, Dendritic voltage recording with transients generated in response to 300 msec current injections through the dendritic recording electrode under control conditions and in the presence of 3 mM CsCl (*C*). *B*, Somatic voltage recording with transients generated in response to 300 msec current injections through the somatic recording electrode under control conditions and in the presence of 3 mM CsCl (*D*). All traces are from dual simultaneous whole-cell recordings from the soma and dendrites (~255 μm) of the same cell. Current injections were −200, −100, −20, −10, +10, +50, +100, and +200 pA. *E*, *F*, Current–voltage relationships for the dendritic (*E*) and somatic (*F*) recordings that are shown *above*. The *lines* are linear regressions of data points for −20, −10, +10, and +50 pA current injections. Note that dendritic R_{in} is much lower than somatic R_{in} under control conditions and that Cs^+ increases dendritic R_{in} a greater amount so that the initial difference between soma and dendrite is nearly removed.

with distance (see Figs. 8, 9*C*, *open squares*). The rate of this decrease is very similar to the decrement of the voltage signal generated by somatic current injection as it propagates into the dendrites (termed the *propagated* dendritic signal; Fig. 9*C, open diamonds*). The result is that the ratio of the two signals (propagated-to-local) is maintained fairly constantly across the dendritic axis (92 ± 2%, $n = 10$; this value does not change with distance, so recordings ranging from 175 to 325 μm were averaged) (see Fig. 9*D, open circles*). Thus, the final amplitude of a voltage signal generated by a current injection (300 msec) into the *dendrite* is almost identical to the final amplitude of a voltage signal generated by the same current injection into the *soma*. The opposite is true when recording from the soma, where the ratio of the somatic voltage change in response to dendritic versus somatic current injection (propagated-to-local signal) decreases as the dendritic injection site is moved distally (from 77 ± 6% at 200 μm, $n = 4$, to 46 ± 6%, $n = 3$, at 300 μm) (Fig. 9*D, open triangles*). External Cs^+ (3 mM) reduces all regional differences in signal propagation, making both the somatic and dendritic propagated-to-local signal ratios decrease as the dendritic recording site is moved farther away from the soma (Fig. 9*B,D, filled circles* and *triangles*).

The effect is that for any given slow (>100 msec) current injection the voltage change occurring at a dendritic location will be the same regardless of whether the current was injected at the dendrite or at a more proximal region. Under conditions of I_h blockade the amplitude of the local dendritic signal decreases very little (Fig. 9*C, filled squares*) with distance so that now the filtering experienced by the propagated signal is greater than the decrease in the local signal (Fig. 9*C, filled diamonds*). The result is a distance-dependent propagated-to-local signal ratio that eliminates this unique form of amplitude normalization (in that it's proximal to distal) provided by the spatial gradient of dendritic I_h (Fig. 9*D, filled circles*).

Kinetics of voltage changes

The membrane charging and discharging rates for voltage deflections spanning a range from +15 to −20 mV were faster in the dendritic compartment when compared with the somatic. The decay of ~10 mV, 50 msec membrane depolarizations could be well fit by single exponential functions (at least an initial period of the decay), and the mean time constant (τ_{mem}) recorded for the

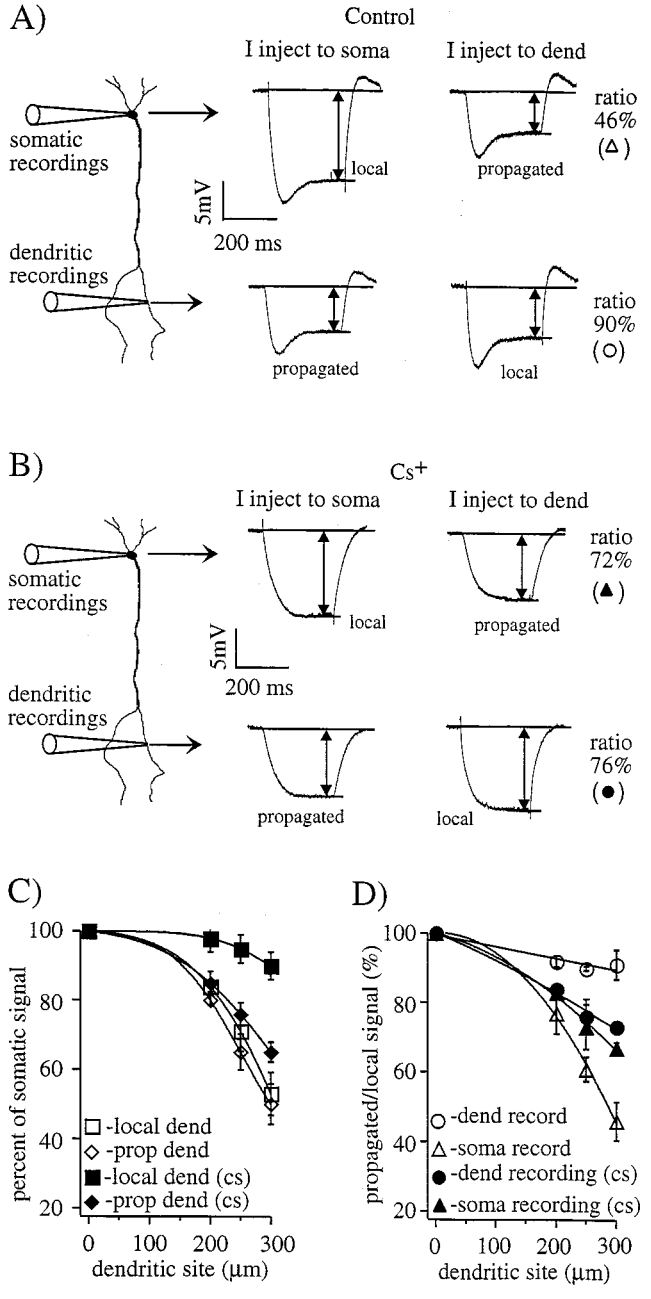

Figure 9. I_h shapes subthreshold voltage propagation. *A*, Simultaneous whole-cell voltage recordings under control conditions from the soma (*top*) and dendrites (*bottom*) of the same neuron in response to somatic (*left column*) and dendritic (*right column*) current injections (−200 pA, 300 msec). To the *extreme right* are the ratios of propagated-to-local signal amplitude for somatic (*top*) and dendritic recordings (*bottom*). Note that in the dendritic recordings (*lower traces*) the final amplitude of the propagated signal (*lower left*) is very similar (90%) to that produced by local current injection (*lower right*). This is not the case for the somatic recordings (*upper traces*). *B*, Simultaneous whole-cell voltage recordings with 3 mM CsCl in bath. In Cs^+, current injections were −100 pA for 300 msec to maintain a 5–10 mV voltage change. *C*, Plot of local and propagated voltage changes occurring with distance from the soma. Local signals are voltage changes recorded at the site of current injection and are expressed relative to the somatic voltage change for somatic current injection (*open squares* in control and *filled squares* in Cs^+). Propagated signals are voltage changes recorded at a site distal to the current injection and also are expressed relative to the local somatic voltage change (*open diamonds* in control and *filled diamonds* in Cs^+). *Data points* are fit arbitrarily by Gaussian functions. *D*, Plot of the ratio of propagated-to-local voltage changes occurring with distance from the soma. From the dendritic recording site (*open circles* in control and *filled circles* in Cs^+), the propagated-to-local signal ratios are the amplitude of the dendritic voltage change in response to *somatic* current injection divided by the amplitude of the dendritic voltage change in response to a *dendritic* current injection. From the somatic recording site (*open triangles* in control and *filled triangles* in Cs^+), the propagated-to-local signal ratios are the amplitude of the somatic voltage change in response to *dendritic* current injection divided by the amplitude of the somatic voltage change in response to a *somatic* current injection. All points are expressed as relative to the local somatic voltage signal and are plotted with respect to the location of the dendritic recording site. *Data points* are fit arbitrarily by polynomial functions, except for control dendritic recordings, which are fit with a *line*.

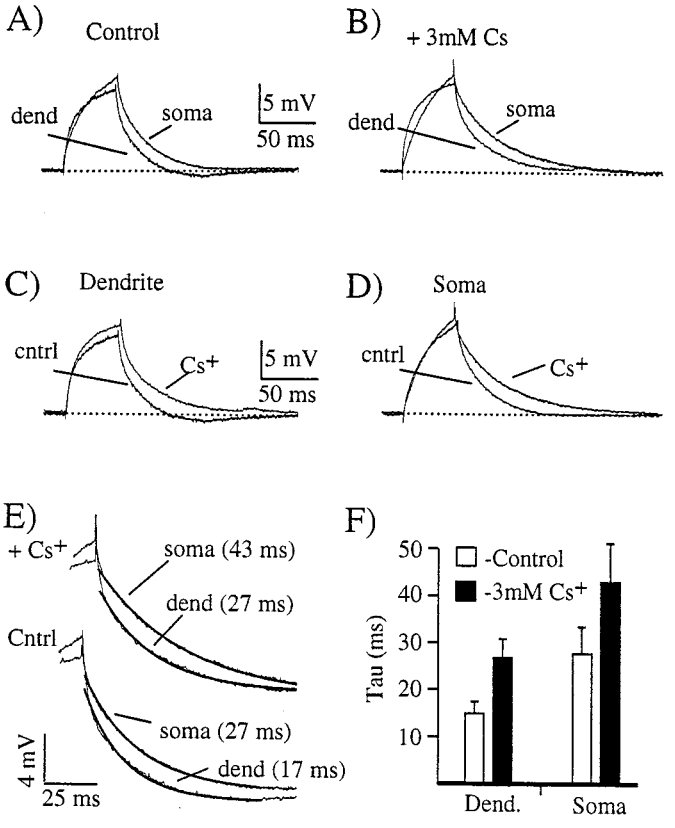

Figure 10. I_h contributes to a faster dendritic membrane charging rate. Shown are somatic and dendritic voltage transients (200 pA, 50 msec) under control conditions (*A*) and with external 3 mM CsCl (*B*). The same traces are grouped by location, showing the slowing effect of 3 mM CsCl on the dendritic (*C*) and somatic compartments (*D*). *E*, Expanded traces from *A* and *B* showing voltage relaxations and their fits by single exponential functions. Note that dendritic repolarization is faster than that observed at the soma even in the presence of 3 mM CsCl. *F*, Plot of repolarization time constants for control conditions (*open bars*; $n = 5$) and in the presence of 3 mM CsCl (*filled bars*; $n = 5$).

dendritic compartments was 15 ± 2 msec as compared with 28 ± 4 msec for somata of the same neurons ($n = 6$; Fig. 10).

In the dendritic compartment a small (1–2 mV) hyperpolarization was observed after the 50 msec depolarizations, whereas no such potential was observed after 50 msec, 10 mV depolarizations in the soma (Fig. 10). These hyperpolarizations were voltage- as well as time-dependent such that the amplitude increased with increasing depolarization and step duration. Significant hyperpolarizations (as well as the depolarizing counterpart; see Fig. 8)

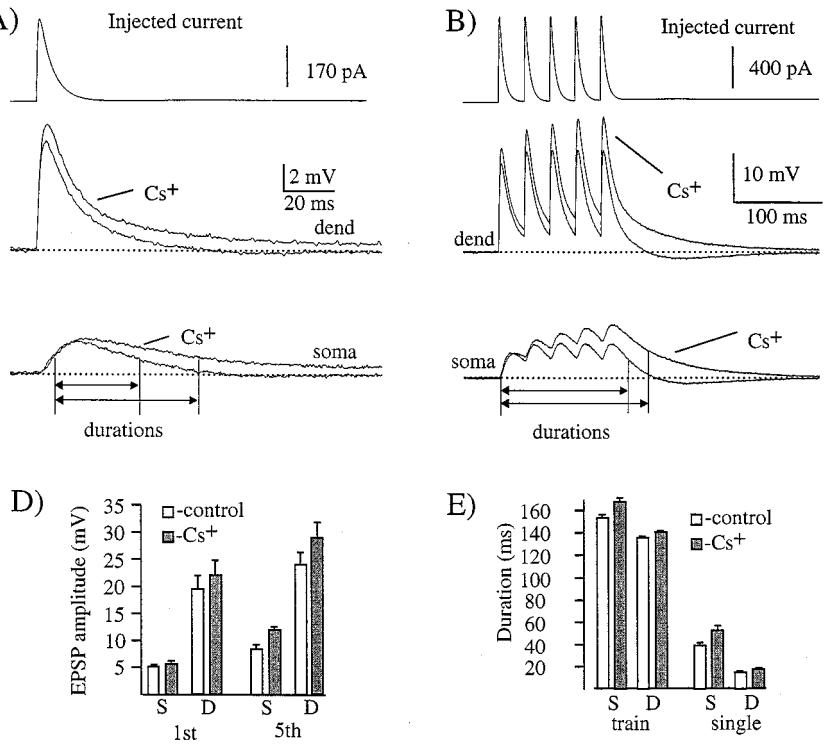

Figure 11. EPSP amplitude, duration, and summation are all regulated by I_h. *A*, A single exponential current injection (340 pA, τ_{rise} = 2 msec and τ_{decay} = 20 msec) into the dendrite (250 μm) produced an EPSP-shaped voltage transient, the amplitude and duration of which were increased in 3 mM CsCl. Attenuation of the single EPSP-shaped transients was similar in both control and Cs^+ conditions (63 ± 3% vs 64 ± 4%, respectively; n = 6). *B*, Repetitive exponential current injections (5–790 pA) produced a train of EPSP-shaped voltage transients, the peak amplitude and duration of which also were increased in 3 mM CsCl. Attenuation of the EPSP-shaped voltage trains was reduced slightly in the presence of external Cs^+ when compared with control (58 ± 5% vs 64 ± 5%, respectively; n = 6). *D*, Pooled data for the somatic (*S*) and dendritic (*D*) EPSP amplitudes for the first and fifth current injections during a train under control conditions (*open bars*) and in the presence of 3 mM CsCl (*filled bars*). *E*, Pooled data for the somatic (*S*) and dendritic (*D*) EPSP durations for trains and single current injections under control conditions (*open bars*) and in the presence of 3 mM CsCl (*filled bars*).

could be observed in the somatic compartment only after longer duration (300 msec) steps. The hyperpolarizations result from I_h channel deactivation during depolarization and subsequent slow channel activation, whereas the depolarizations after negative current injection are, conversely, the result of the slow I_h deactivation rate (Mayer and Westbrook, 1983; Spain et al., 1987; Schwindt et al., 1988; McCormick and Pape, 1990).

Application of external Cs^+ (3 mM) increased τ_{mem} in both the somatic and dendritic compartments and eliminated the hyperpolarization normally observed after the 50 msec depolarizations. However, regional differences in τ_{mem} were still present under I_h blockade, with the dendritic compartment remaining faster (dendrite, 27 ± 5 msec; soma, 42 ± 10 msec; n = 6) (Fig. 10). These data suggest that, although I_h participates in setting both R_{in} and τ_{mem} (at least in terms of 5–10 mV transients), other factors also are involved in setting a faster τ_{mem} in the dendritic compartment even in the absence of substantial I_h. Such factors could be nonuniformities in membrane resistivity (R_m) or in other ionic channel populations (Drake et al., 1997; Hoffman et al., 1997; Stuart and Spruston, 1998) Also, the incomplete I_h blockade by 3 mM Cs^+ could account for part of the remaining regional differences (see also Fig. 8).

EPSP integration

Because of the prominent role that I_h plays in setting both R_{in} and τ_{mem}, the impact of I_h on the summation of synaptic activity was tested directly by using dendritic current injections. Under control conditions, exponential current injections (τ_{rise} = 2 msec; τ_{decay} = 20 msec) into the dendritic compartment resulted in EPSP-shaped voltage transients, the amplitude and kinetics of which were filtered significantly as they propagated from the dendritic injection site to the somatic recording site (dendritic amplitude, 8 ± 0.5 mV; dendritic duration, 15 ± 0.8 msec; somatic amplitude, 3 ± 0.2 mV; somatic duration, 39 ± 2 msec) (Fig. 11*A,D,E*). Repetitive current injections also were given to mimic repetitive synaptic input, and these events were filtered similarly by the dendritic arborizations (dendritic amplitude, 24 ± 3 mV; dendritic duration, 136 ± 1 msec; somatic amplitude, 8 ± 1 mV; somatic duration, 154 ± 2 msec) (Fig. 11*B,D,E*). As with step depolarizations, a slight hyperpolarization was generated (particularly in the dendrites) after EPSP depolarization. The amplitude of this hyperpolarization was larger after trains of input (<5 mV) than for single EPSPs (<2 mV).

I_h channel blockade increased both single EPSP amplitude (soma, 10 ± 2%; dendrite, 7 ± 4%) and duration (soma, 38 ± 9%; dendrite, 10 ± 2%) as well as repetitive EPSPs amplitude (soma, 42 ± 8%; dendrite, 22 ± 5%) and duration (soma, 7 ± 2%; dendrite, 3 ± 1%) (Fig. 11). Although the peak amplitude of *single* EPSPs increased only slightly in Cs^+, the increase was fairly uniform in both the soma and the dendrites such that the amount of amplitude attenuation occurring between the dendrites and soma was unaffected by I_h blockade (control was 63 ± 3% vs 64 ± 4% in Cs^+). On the other hand, the peak amplitude reached during EPSP *trains* increased twice as much in the soma as in the dendrite; thus, for repetitive activity the amount of attenuation occurring between the dendrites and soma was reduced by I_h blockade (control was 66 ± 5% vs 58 ± 6% in Cs^+).

Under conditions of I_h blockade the increased amplitude of single somatic EPSPs is mostly the result of an elevation in effective R_{in}, whereas the more pronounced effect on EPSP duration results from both the increased R_{in} and τ_{mem}. Because the amount of summation occurring during repetitive activity is dependent on both effective R_{in} and τ_{mem}, the effect of Cs^+ on the peak amplitude reached during an EPSP train is more pronounced than for single EPSPs. Presumably, the slight improvement in the propagation of EPSP trains and not single EPSPs during the blockade of I_h reflects the involvement of both R_{in} and τ_{mem}.

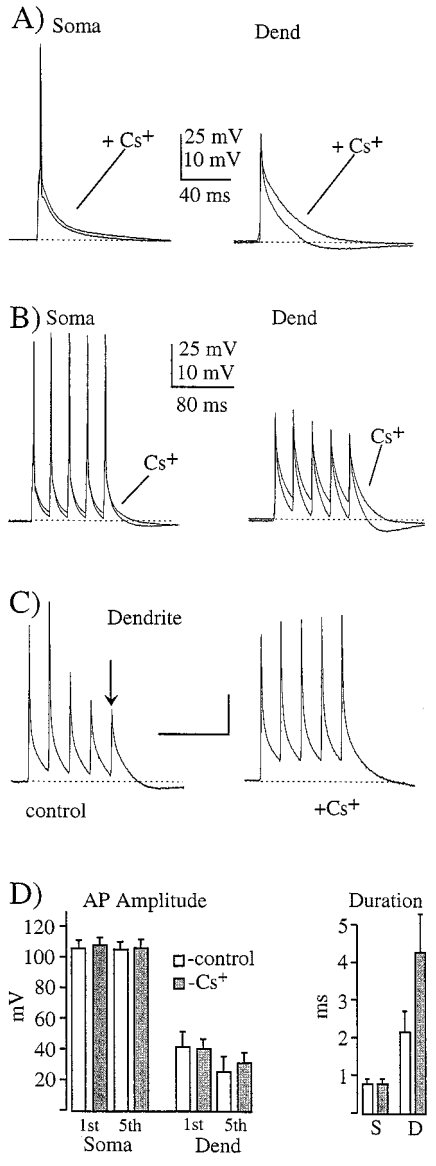

Figure 12. Action potential backpropagation is affected only slightly by dendritic I_h. *A*, Dual whole-cell recordings from the soma and dendrite (~290 μm) with a single action potential evoked by a suprathreshold exponential current injection into the soma (1.2 nA). I_h blockade does not improve dendritic action potential propagation but does slow the more hyperpolarized components of repolarization in both the soma and dendrite. *B*, In the same cell the propagation of short trains (30 Hz) of action potentials likewise was unaffected by Cs^+. The rates of membrane repolarization between the spikes and a prominent dendritic afterhyperpolarization are, however, all reduced by I_h blockade. Similar results also were observed for 15 Hz trains. *C*, In some cells (two of six) the frequency dependence of action potential amplitude was reduced by external 3 mM CsCl. *D*, Pooled data for somatic and dendritic action potential amplitude (*1st* and *5th* spikes in the train) and duration (single spikes; *S*, somatic; *D*, dendritic) under control conditions (*open bars*) and in the presence of 3 mM CsCl (*filled bars*).

Action potential backpropagation

The backpropagation of action potentials was affected only slightly by I_h blockade, with the most consistent effect being on the more hyperpolarized regions of the repolarization phase (Fig. 12). The amplitudes of single somatic and dendritic action potentials were not changed by I_h blockade (soma: 101 ± 4 to 103 ± 5 mV, $n = 6$; dendrite: 42 ± 9 to 41 ± 9 mV, $n = 6$), whereas the duration (at half-maximum amplitude) of dendritic action potentials was prolonged considerably by external Cs^+ (dendrite: 2.2 ± 0.5 to 4.4 ± 1.3 msec, $n = 6$). In the dendrites, single action potentials and particularly trains of multiple action potentials generally were followed by an afterhyperpolarization (AHP) (1–2 mV), a component of which was sensitive to external Cs^+ (Fig. 12). This suggests that I_h deactivation occurring during action potentials significantly contributes to dendritic spike repolarization, particularly in the −40 to −65 mV range (Spain et al., 1987; Schwindt et al., 1988; Maccaferri et al., 1993). In a minority of cases (two of six neurons), I_h blockade reduced the amount of amplitude attenuation occurring during a train of five dendritic action potentials, and in these two neurons the accompanying decrease in the action potential maximum rate of rise was reduced also. Thus the dampening effect of dendritic I_h does appear to increase the susceptibility of the dendrites to frequency-dependent action potential backpropagation, perhaps by lowering R_{in} and by providing a mechanism for dendritic AHP generation.

DISCUSSION

Hyperpolarization-activated currents were found throughout the entire extent of CA1 pyramidal neurons presently studied (soma to 350 μm of apical dendrite). These currents displayed a biophysical and pharmacological profile that is most characteristic of the current termed I_h. Generally speaking, the ionic selectivity, voltage ranges of activation, and kinetics of activation and deactivation as well as the sensitivity to external Cs^+ all fall within the ranges reported for a wide variety of central and peripheral neurons as well as cardiac cell types (DiFrancesco, 1981; Halliwell and Adams, 1982; Mayer and Westbrook, 1983; Spain et al., 1987; McCormick and Pape, 1990; Maccaferri et al., 1993). The presence of a significant dendritic I_h density acts to lower the R_{in} of the dendritic compartment as well as to speed the kinetics of membrane polarization. These alterations in basic dendritic membrane properties impact both the shape and propagation of sub- and suprathreshold electrical signals.

Channel distribution

An increase in I_h density was found across the somatodendritic axis such that the density of the most distal regions was nearly sevenfold larger than that in the somatic region. A similar nonuniform channel density has been reported for a transient K^+ current in CA1 pyramidal neurons, whereas Na^+ and composite Ca^{2+} current density remains relatively constant from soma to distal apical dendrite (Magee and Johnston, 1995; Hoffman et al., 1997). Very recently, the products of several cloned genes have been shown to produce hyperpolarization-activated currents that are characteristically similar to I_h, and corresponding RNA has been found in abundance in the hippocampus (Santoro et al., 1997; Gauss et al., 1998; Ludwig et al., 1998; Santoro et al., 1998). Unfortunately, extensive channel labeling or binding studies are not yet available to corroborate the presence of these channels in the dendritic arbors of CA1 pyramidal neurons. However, the presence of a greatly elevated membrane sag during hyperpolarizations (a classic hallmark of I_h) has been reported in several intradendritic recording studies from at least two different pyramidal cell types (Andreasen and Lambert, 1995; Tsubokawa and Ross, 1996; Stuart and Spruston, 1998). In fact, an elevated dendritic I_h density was required for the realistic neuronal model of Stuart and Spruston (1998) to match whole-cell data recorded from the soma and dendrites of neocortical pyramidal neurons.

The data presented here support the hypothesis that a nonuniform density of I_h exists in cortical pyramidal neurons.

Even with the elevated dendritic I_h densities, absolute I_h density is quite small when compared with other dendritic channel densities, Na^+ and K^+ channels in particular. Despite being a relatively small conductance, the persistent nature of this current, as well as the voltage dependence of its activation range, determines that I_h current amplitudes are sufficient to impact profoundly most aspects of subthreshold dendritic membrane activity.

Activation voltage ranges

The observed hyperpolarized shift (~10 mV) in the voltage range of activation for I_h channels located in more distal regions is possibly the result of differential levels of channel modulation between the distal and proximal regions of the CA1 pyramidal neurons. The I_h activation curve is reportedly very sensitive to intracellular adenylate cyclase and cAMP activities. Increases in cAMP (such as observed during β-receptor activation) lead to depolarizing shifts, whereas decreases (such as during muscarinic receptor activation) shift the curve in a more hyperpolarized direction (Ingram and Williams, 1996; Pape, 1996; Jafri and Weinreich, 1998). A similar hyperpolarized shift in the voltage range of activation also has been reported for a transient K^+ current located in the distal dendrites of CA1 pyramidal neurons (Hoffman et al., 1997). These channels likewise are sensitive to cAMP levels (Hoffman and Johnston, 1998). Taken together, it seems probable that the shift in the I_h activation curve could be the result of a lower basal level of cAMP activity in the more distal regions of CA1 pyramidal dendrites. Because the shift in the voltage range of activation of transient K^+ current ultimately appears to be regulated by phosphorylation by PKA, an increased phosphatase activity also could be involved in this modulation. However, such regulation by phosphorylation does not appear to be involved in the shifting of I_h activation ranges (Pedarzani and Storm, 1995); therefore, the simplest explanation is that a lower resting cAMP activity results in a hyperpolarized shift in the I_h activation curve for channels located in the more distal regions of the dendritic arbor.

Functional impact of dendritic I_h

The major impact of the elevated dendritic density of I_h channels is a decreased apparent R_{in} and a faster τ_{mem} in the dendritic compartment. As a result of these effects, membrane depolarizations and, to an even greater extent, hyperpolarizations are increasingly blunted the more distal one proceeds across the somatodendritic axis. Therefore, the absolute effectiveness of more distal synaptic input (i.e., the total charge transferred from synapse to soma) will be reduced by the increasingly large I_h conductance. A similar situation appears to be present in neocortical pyramidal neurons, where I_h has been shown to decrease the current transmitted from the dendrites to the soma for both EPSPs and more prolonged input (Schwindt and Crill, 1997; Stuart and Spruston, 1998). The lowered dendritic R_{in} and τ_{mem} also act to reduce the amount of summation that occurs during repetitive synaptic activation. Such an effect will reduce the time window over which temporal summation and coincidence detection can occur, allowing higher frequency input to be discriminated (Banks et al., 1993; Shadlen and Newsome, 1994; Softky, 1995; Hausser and Clark, 1997).

The spatial gradient of I_h determines that the amplitude decrement exhibited by slower voltage signals as they propagate from the soma into the dendrites is strikingly similar to the distance-dependent decrease in the amplitude of local voltage signals. Because of this, a form of amplitude normalization occurs where, for example, slow inhibitory synaptic input into the proximal regions would have almost exactly the same impact on the distal dendritic compartments as would inhibitory input that was received locally in the distal dendrites themselves. The opposite effect will occur for the impact of slow input into the dendrites on the somatic compartment. In this case the spatial gradient of I_h causes inhibition to the dendrites to have a much reduced impact on the soma as compared with that received by somatic inhibition. Thus, proximal slow polarization events (such as repetitive ~5 Hz inhibitory input observed during theta activity) will impact the dendritic integration of synaptic input with almost exactly the same efficacy as distally arriving events.

Although the impact of I_h on subthreshold voltage events is more obvious than on action potential propagation, the general membrane-shunting effect of I_h and the generation of AHPs determine that I_h does act, along with the transient K^+ current, to reduce the excitability of dendritic membrane. In fact, without I_h the more distal dendrites do not appear to contain any mechanism for generating AHPs. Although the primary regulator of dendritic excitability remains the large transient K^+ current present in the distal dendrites, the elevated I_h density does have an additional blunting effect, particularly where trains of action potentials are concerned. In fact, the muscarinic modulation of spike backpropagation observed in hippocampal CA1 neurons may be attributable in part to the inhibitory effects of muscarinic receptor activation on I_h (Tsubokawa and Ross, 1997).

As discussed above, the voltage range of I_h activation is extremely modulatable (Pape, 1996). The hyperpolarized voltage range of activation observed in the more distal dendrites under basal slice conditions lowers the impact of these channels, whereas the elevated density provides the potential for an even greater impact on all of the properties discussed above. Thus, the influence of the elevated dendritic I_h density on the resting membrane potential, the integration of synaptic input, and action potential propagation are all highly dependent on the modulatory state of the I_h channels.

Overall, I_h acts to dampen dendritic excitability in much the same way as the transient K^+ current found in high density in CA1 dendrites. However, in contrast to dendritic K^+ currents I_h has its largest impact on the subthreshold range of membrane potentials where the integration of inhibitory and excitatory synaptic inputs takes place. Because of the prominent role that I_h plays in the determination of basic membrane properties and the susceptibility of I_h to modulation, the manner in which synaptic potentials are integrated within the dendritic arborization can be altered easily and effectively during different physiological conditions.

REFERENCES

Andreasen M, Lambert JDC (1995) Regenerative properties of pyramidal cell dendrites in area CA1 of the rat hippocampus. J Physiol (Lond) 483:421–441.

Banks MI, Pearce RA, Smith PH (1993) I_h in neurons of the medial nucleus of the trapezoid body: voltage-clamp analysis and enhancement by norepinephrine and cAMP suggest a modulatory mechanism in the auditory brainstem. J Neurophysiol 70:1420–1432.

Byerly L, Chase PB, Stimers JR (1984) Calcium current activation kinetics in neurones of the snail *Lymnaea stagnalis*. J Physiol (Lond) 348:187–207.

DiFrancesco D (1981) A study of the ionic nature of pace-maker current in calf Purkinje fibers. J Physiol (Lond) 314:377–393.

DiFrancesco D (1986) Characterization of single pacemaker channels in cardiac sino-atrial cells. Nature 324:470–473.

Drake CT, Bausch SB, Milner TA, Chavkin C (1997) GIRK1 immunoreactivity is present predominantly in dendrites, dendritic spines, and somata in the CA1 region of the hippocampus. Proc Natl Acad Sci USA 94:1007–1012.

Gasparini S, DiFrancesco D (1997) Action of the hyperpolarization-activated current blocker ZD7288 in hippocampal neurons. Pflügers Arch 435:99–106.

Gauss R, Seifert R, Kaupp UB (1998) Molecular identification of a hyperpolarization-activated channel in sea urchin sperm. Nature 393:583–587.

Halliwell JV, Adams PR (1982) Voltage-clamp analysis of muscarinic excitation in hippocampal neurons. Brain Res 250:71–92.

Hausser M, Clark B (1997) Tonic synaptic inhibition modulates neuronal output pattern and spatiotemporal synaptic integration. Neuron 19:665–678.

Haverkampf K, Benz I, Kohlhardt M (1995) Thermodynamically specific gating kinetics of cardiac mammalian K^+(ATP) channels in a physiological environment near 37°C. J Membr Biol 146:85–90.

Hille B (1992) Ionic channels of excitable membranes, p 376. Sunderland, MA: Sinauer.

Hoffman DA, Johnston D (1998) Downregulation of transient K^+ channels in dendrites of hippocampal CA1 pyramidal neurons by activation of PKA and PKC. J Neurosci 18:3521–3528.

Hoffman DA, Magee JC, Colbert CM, Johnston D (1997) K^+ channel regulation of signal propagation in dendrites of hippocampal pyramidal neurons. Nature 387:869–875.

Ingram SL, Williams JT (1996) Modulation of the hyperpolarization-activated current (I_h) by cyclic nucleotides in guinea-pig primary afferent neurons. J Physiol (Lond) 492[Pt 1]:97–106.

Jafri MS, Weinreich D (1998) Substance P regulates I_h via NK-1 receptor in vagal sensory neurons of the ferret. J Neurophysiol 79:769–777.

Ludwig A, Zong XG, Jeglitsch M, Hofmann F, Biel M (1998) A family of hyperpolarization-activated mammalian cation channels. Nature 393:587–591.

Maccaferri G, McBain CJ (1996) The hyperpolarization-activated current and its contribution to pacemaker activity in rat CA1 stratum oriens–alveus interneurons. J Physiol (Lond) 497:119–130.

Maccaferri G, Mangoni M, Lazzari A, DiFrancesco D (1993) Properties of the hyperpolarization-activated current in rat hippocampal CA1 neurons. J Neurophysiol 69:2129–2136.

Magee JC, Johnston D (1995) Characterization of single voltage-gated Na^+ and Ca^{2+} channels in apical dendrites of rat CA1 pyramidal neurons. J Physiol (Lond) 487:67–90.

Magee JC, Avery RB, Christie BR, Johnston D (1996) Dihydropyridine-sensitive, voltage-gated Ca^{2+} channels contribute to the resting intracellular Ca^{2+} concentration of hippocampal CA1 pyramidal neurons. J Neurophysiol 76:3460–3470.

Magee JC, Hoffman D, Colbert C, Johnston D (1998) Electrical and calcium signaling in dendrites of hippocampal pyramidal neurons. Annu Rev Physiol 60:327–346.

Maruoke F, Nakashima Y, Takano M, Ono K, Noma A (1994) Cation-dependent gating of the hyperpolarization-activated current in the rabbit sino-atrial node cells. J Physiol (Lond) 477[Pt 3]:423–435.

Mayer ML, Westbrook GL (1983) A voltage-clamp analysis of inward (anomalous) rectification in rat sensory ganglion neurons. J Physiol (Lond) 375:327–338.

McAllister-Williams RH, Kelly JS (1995) The temperature dependence of high-threshold calcium channel currents recorded from adult rat dorsal raphe neurones. Neuropharmacology 34:1479–1490.

McCormick DA, Pape HC (1990) Properties of a hyperpolarization-activated cation current and its role in rhythmic oscillation in thalamic relay neurons. J Physiol (Lond) 431:319–342.

Milburn T, Saint DA, Chung SH (1995) The temperature dependence of conductance of the sodium channel: implications for mechanisms of ion permeation. Receptors Channels 3:201–211.

Pape HC (1996) Queer current and pacemaker: the hyperpolarization-activated cation current in neurons. Annu Rev Physiol 58:299–327.

Pape HC, McCormick DA (1989) Noradrenaline and serotonin selectively modulate thalamic burst firing by enhancing a hyperpolarization-activated current. Nature 340:715–718.

Pedarzani P, Storm JF (1995) Protein kinase A-independent modulation of ion channels in the brain by cyclic AMP. Proc Natl Acad Sci USA 92:11716–11720.

Santoro B, Grant SGN, Bartsch D, Kandel E (1997) Interactive cloning with the SH3 domain of N-src identifies a new brain-specific ion channel protein, with homology to *eag* and cyclic nucleotide-gated channels. Proc Natl Acad Sci USA 94:14815–14820.

Santoro B, Liu DT, Yao H, Bartsch D, Kandel E, Siegelbaum SA, Tibbs GR (1998) Identification of a gene encoding a hyperpolarization-activated pacemaker channel of brain. Cell 93:717–729.

Schwindt PC, Crill WE (1997) Influence of anomalous rectifier on afterhyperpolarizations of neurons from cat sensorimotor cortex *in vitro*. J Neurophysiol 78:187–198.

Schwindt PC, Spain WJ, Crill WE (1988) Modification of current transmitted from apical dendrites to soma by blockade of voltage- and calcium-dependent conductances in rat neocortical neurons. J Neurophysiol 59:468–481.

Shadlen M, Newsome WT (1994) Noise, neural codes, and cortical organization. Curr Opin Neurobiol 4:569–579.

Softky W (1995) Simple codes versus efficient codes. Curr Opin Neurobiol 5:239–247.

Spain WJ, Schwindt PC, Crill WE (1987) Anomalous rectification in neurons from cat sensorimotor cortex. J Neurophysiol 57:1555–1576.

Stuart G, Spruston N (1998) Determinates of voltage attenuation in neocortical pyramidal neuron dendrites. J Neurosci 18:3501–3510.

Stuart G, Spruston N, Sakmann B, Hausser M (1997) Action potential initiation and backpropagation in neurons of the mammalian CNS. Trends Neurosci 20:125–131.

Tsubokawa H, Ross WN (1996) IPSPs modulate spike backpropagation and associated $[Ca^{2+}]_i$ changes in the dendrites of hippocampal CA1 pyramidal neurons. J Neurophysiol 76:2896–2906.

Tsubokawa H, Ross WN (1997) Muscarinic modulation of spike backpropagation in the apical dendrites of hippocampal CA1 pyramidal neurons. J Neurosci 17:5782–5791.

van Lunteren E, Elmslie KS, Jones SW (1993) Effects of temperature on calcium current of bullfrog sympathetic neurons. J Physiol (Lond) 466:81–93.

Wollmuth LP (1995) Multiple binding sites in I_h channels of rod photoreceptors from tiger salamanders. Pflügers Arch 430:34–43.

Yuste R, Tank DW (1996) Dendritic integration in mammalian neurons, a century after Cajal. Neuron 16:701–716.